Ordered Transmembrane and Extracellular Structure in Squid Photoreceptor Microvilli

Helen Saibil and Elizabeth Hewat

Zoology Department, University of Oxford, Oxford OX1 3PS, United Kingdom

Abstract. Invertebrate retinas contain hexagonal arrays of microvilli that form the honeycomb structure of rhabdome photoreceptors. The largest and most crystalline rhabdomes are found in the squid retina, and we have taken advantage of their unique properties to derive a model for the electron density distribution in microvillar membranes using low angle X-ray diffraction combined with correlation averaging of electron microscope images. The model electron density map, calculated to a resolution of ~35 Å, shows an unusually high protein content in the membranes. This may be associated with a dense meshwork of membrane junctions between neighboring microvilli as revealed by electron microscope image analysis. Membrane pair contacts are resolved as two or more strands of density crossing the membranes. The microvilli are also linked together by Y-shaped junctions at their three-way contacts. These two sorts of junctions link the membranes into a three-dimensional array and partition them into a mosaic of deformable and rigid domains. This arrangement maintains a remarkable degree of long-range order in squid rhabdomes, and may be responsible for the alignment of rhodopsin molecules. The structural order observed is necessary for these photoreceptors to achieve their high sensitivity to the plane of polarized light. Rhodopsin constitutes about one-half the microvillar protein. The remaining proteins, which can be divided into approximately equal detergent-soluble and insoluble fractions, could account for the composition of the new structures described.

THE photoreceptors in the squid retina possess a high degree of structural order at the cellular, subcellular, and molecular levels. They consist of microvilli, which are cylindrical extensions of the cell membrane, packed hexagonally into a honeycomb structure characteristic of invertebrate rhabdomes. The microvilli are 600 Å in diameter and 1-μm long, and they are stacked transversely in bundles 200–300-μm high. The arrangement of retinula cells in the retina and of microvilli within the rhabdomes are shown in the diagram of Fig. 1. The microvillus membrane is the focus of an orderly series of attachments from the actin-containing cytoskeleton in the microvillar cytoplasm and from a network of membrane contacts between neighbors on the extracellular surface (18). The microvilli contain a predominant integral membrane protein, the visual pigment rhodopsin, in addition to 8–10 other prominent polypeptides.

Retinal photoreceptors absorb light and convert it into fluctuations of membrane potential, which are then transmitted via the optic nerve to the brain. The biochemical transduction mechanisms of these processes are conserved between vertebrates and invertebrates, and homologies in rhodopsin primary structure have been found between *Drosophila* and vertebrate rhodopsin (14). Photoexcited rhodopsin molecules activate membrane-associated enzymes which in turn regulate the concentrations of cytoplasmic messenger substances. In the rod outer segment (ROS)[1] disk membrane of vertebrates, each rhodopsin molecule can activate many GTP-binding proteins while diffusing laterally in the plane of the membrane. These in turn activate the cyclic guanosine monophosphate (GMP) phosphodiesterase, lowering cyclic GMP, and hyperpolarizing the cell membrane (reviewed in 25). In contrast to ROS, which contain little cytoskeleton (17) and possess a freely diffusing rhodopsin, invertebrate photoreceptors in species with high polarization sensitivity (such as squid and crayfish) have a precisely organized structure in which the rhodopsin chromophores are aligned parallel to the microvillar axis. Lattices of membrane particles have been observed in photoreceptor microvilli by freeze fracture electron microscopy and have been attributed to rhodopsin (3, 5). Although immobile, squid rhodopsin also activates a GTP-binding protein (20, 28, 31). This may mediate an increase in cyclic GMP (10, 19) and/or the hydrolysis of phosphatidylinositol bisphosphate (27, 32, 35), resulting in depolarization of the retinula cell membrane.

In this paper we describe ordered transmembrane and extracellular structures which form two types of contact be-

Dr. Hewat's present address is Laboratoire d'Eléctronique et de Technologie de l'Informatique, Centre d'Etudes Nucléaires de Grenoble, 85X, 38041 Grenoble, France.

1. *Abbreviation used in this paper*: ROS, rod outer segment.

tween the microvilli. These structures were revealed by combining X-ray diffraction studies with real space correlation averaging of electron microscope images. By using dextrans in the fixation medium to manipulate the osmotic balance in the retina, details of membrane junctions are revealed and shown to be consistent with the X-ray patterns. The composition of the structures described may be accounted for by a small number of nonrhodopsin polypeptides comprising one-half the microvillar protein.

Materials and Methods

Living, active specimens of the small squid *Alloteuthis subulata* were obtained from The Laboratory, Marine Biological Association (Plymouth, UK), and were kept in dim light or darkness in seawater tanks for 6 h–3 d before use. Fixation of the retinas was initiated within 1 min of decapitation. After removal of tentacles and beak, the anterior parts of the eyes were sliced off and the exposed retinas, attached to the intact optic lobes, were immersed in fixative at room temperature. All steps were performed in dim red light or darkness.

X-ray Diffraction

The composition of the fixation medium for the X-ray work was 15% (wt/vol) sucrose, 475 mM NaCl, 10 mM KCl, 20 mM $MgSO_4$, 10 mM EGTA, 25 mM 3-(*N*-morpholino)-propane sulfonic acid (MOPS) pH 7.4, 2% glutaraldehyde. After 1 h of fixation at room temperature, retinas were stored at 0–4°C in the same medium. Glutaraldehyde fixation was necessary because this retinal tissue disintegrates within ≈1 h of dissection. 0.5-mm thick strips of glutaraldehyde-fixed retina were sliced along the axes of the cellular lattice, as shown in Fig. 1. Correctly aligned slices were obtained as previously described (18), and exposed at 4°C in a Franks double mirror camera on a rotating anode generator (model GX-13; Marconi-Elliott Avionic Systems, Borehamwood, Hertshire, UK). The X-ray beam was perpendicular to the long axis of the retinula cells. Patterns were recorded on CEA Reflex 25 X-ray film.

Electron Microscopy

After several hours of glutaraldehyde fixation (EM fixation buffer as for X-ray except that 15% sucrose was replaced by 5% sucrose and 5% dextran of mol wt 10,000 or 73,000), retinas were cut into oriented strips as above. These were washed in fixation buffer, omitting glutaraldehyde, and then osmium fixed on ice for 30 min. The 0.5% OsO_4 in buffer contained 5% dextran, 10% sucrose, and 1/2 the original salt and buffer concentrations. The slices were then washed in water, dehydrated in ethanol, and embedded in LR White resin (hard grade; London Resin Co., Basingstoke, UK). 400–600-Å thick sections (dark to medium gray interference color), cut on a microtome (C. Reichert AG, Vienna, Austria) with a diamond knife, were supported on bare 700-mesh grids and stabilized with a thin carbon layer. Sections were stained with either aqueous uranyl acetate (15 min) and lead citrate (5 min), or with 5% phosphotungstic acid in ethylene glycol for 2 h at 50°C. Specimens were observed in a Philips 400T electron microscope at 80 kV and 36000 or 50000× magnification, and photographed on Ilford EM film.

Image Analysis

Micrographs were digitized with a 50- or 100-μm raster using a Scandig rotating drum microdensitometer coupled to a Datageneral Nova computer

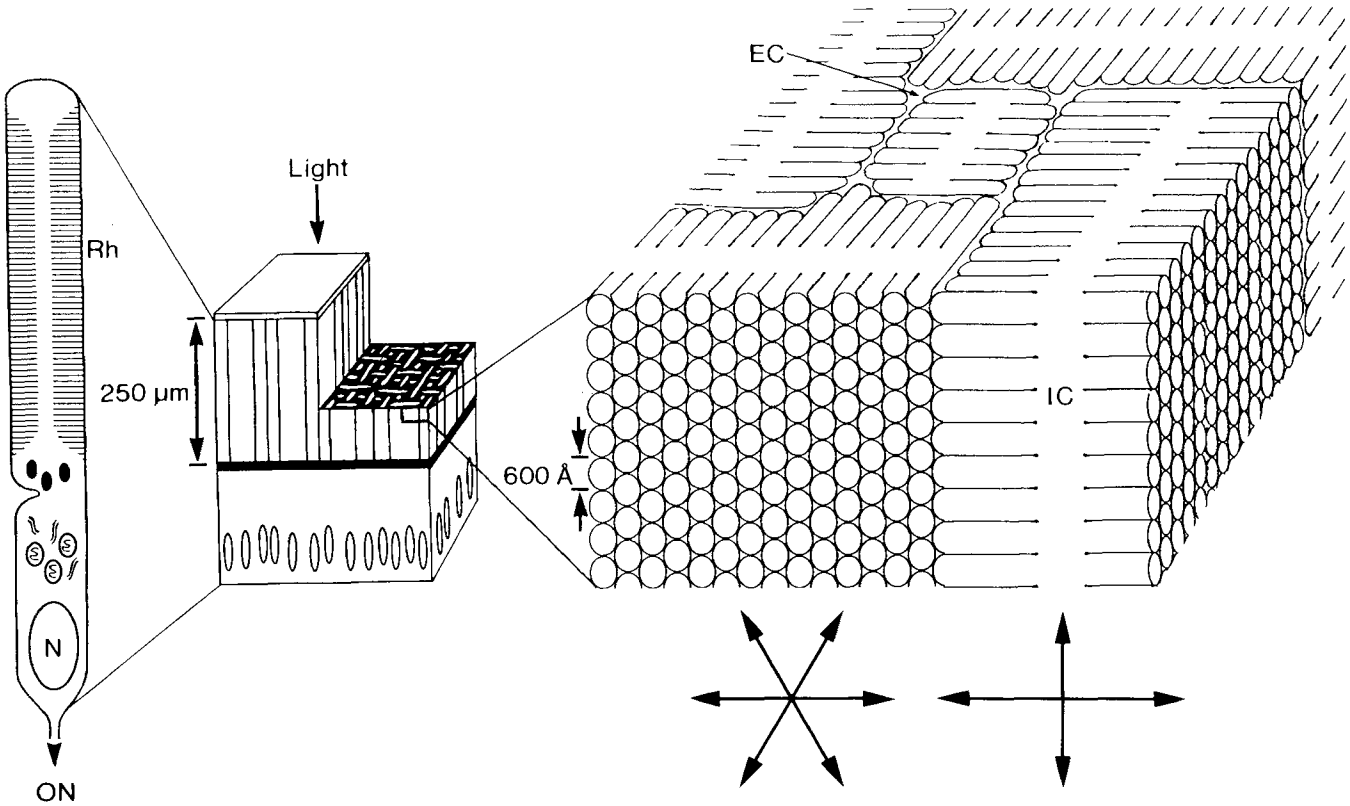

Figure 1. Schematic diagram of a slice of squid retina (*center*) with expanded areas showing the structure of a retinula cell (*left*) and the arrangement of photoreceptor membranes in the rhabdomes (*right*). The photoreceptor layer of the retina (*center, vertical stripes*) faces the incoming light and the cut-away region shows the appearance of the receptor mosaic in transverse section. In longitudinal section, the cells appear variable in width, depending on how the section plane intercepts the cellular mosaic. The retinula cells (*left*) are divided into two segments that are separated by a layer of screening pigment granules. Although the photoreceptors face the interior of the cephalopod camera eye, we refer to them as 'outer segments' by analogy with vertebrate photoreceptor outer segments that face the outside of the eye. Rh, rhabdome; N, nucleus; ON, optic nerve fiber. The ribbon-like outer segments weave together into a retinal mosaic with the microvilli running in two orthogonal directions (*right*). The diffraction axes of these two zones are shown (*bottom, right*). EC, extracellular space; IC, intracellular space.

(Data General Corp., Southboro, MA). The best ordered areas of 512 × 512 pixels, containing 100–200 microvilli, were extracted for analysis. Real space averages of 128 × 128 pixels were produced using the correlation averaging facility of the SEMPER-V system (9, 23) installed on the VAX 11/750 computer of the Oxford Laboratory of Molecular Biophysics. The correlation averaging method (22) was applied as follows: (*a*) A small area (64 × 64 pixels) containing ~1 unit cell is extracted from the digitized micrograph. (*b*) A cross-correlation between the extracted area and the whole image is calculated. This gives a correlation peak at the position of every unit cell resembling the extracted one. (*c*) The positions and heights of the peaks are determined and an average is calculated for an area 128 × 128 pixels centered at each peak above a specified height. (*d*) The resulting averaged area can then be used to derive a new set of correlation peaks, eliminating possible bias from the initial selection, and a new average is calculated. Images averaged by the Fourier technique of filtering the diffraction pattern, which assume a perfect lattice, are degraded by small distortions in the lattice while real space averaging corrects or eliminates distorted regions from the average.

Model Calculations

Using the image creation routines of the SEMPER system, model electron density maps were constructed with the desired membrane density profiles and microvillar shapes, and their diffraction patterns calculated by Fourier transformation. Positions of intensity maxima and minima were measured, and relative intensities compared by eye with the X-ray diffraction data. Our aim was to reproduce the envelope of major intensity maxima and minima in the X-ray patterns so as to find a structure that would account for the observed diffraction data. The microvillus cross section was modeled either as a circle or as a hexagon with rounded corners by joining together six segments of arc (see Fig. 8). The electron density profile of the microvillar membrane was modeled as the sum of three Gaussian distributions, taking the experimentally determined profile of ROS disc membranes (2) as the starting shape (see Fig. 6).

Exactly four unit cells of the model microvilli were extracted into a 256 × 256 pixel file. For ease of computation, different sampling distances were used on the x- and y-axes, giving the 15% stretched hexagonal lattice seen in Fig. 8, *a* and *b*. This was to allow integral sampling of the hexagonal lattice by the rectilinear grid of pixels. Because the unit cell parameters coincide with sampling positions, the squared Fourier transform of this model file gives the sampled diffraction pattern directly (see Fig. 7). For a justification of this procedure see reference 21 (pp. 41–43).

Microvillar Membrane Isolation and Detergent Fractionation

Outer segments were detached from thawed squid retinas and microvillar membranes isolated by sucrose flotation as previously described (20) in 0.4 M NaCl, 20 mM $MgSO_4$, 10 mM EGTA , 20 mM MOPS pH 7.4. The microvillar membranes were washed in 30 mM NaCl, 2 mM $MgSO_4$, 20 mM MOPS pH 7.4, and the detergent extraction was done by gradually mixing the membrane suspension with an equal volume of 4% (wt/vol) octyl glucoside in water. The detergent insoluble fraction was pelleted by centrifugation at 15,000 *g* in a 1.5-ml tube for 5 min. 10% polyacrylamide slab gels (12) were scanned in a densitometer (Joyce, Loebl and Co. Ltd., Gateshead, UK).

Results

X-ray Diffraction of Squid Retina

Low angle X-ray diffraction patterns obtained from slices of glutaraldehyde-fixed retina are shown in Fig. 2. The projection in the beam direction contains two orthogonal sets of microvilli oriented as in Fig. 1 (right). Scattering from the microvilli viewed head-on is along the axes shown for the hexagonal array, while those viewed from the side scatter mainly along the vertical axis (Fig. 1, and see Fig. 2 of reference 18). The discrete spots (Fig. 2 *a*) are due to hexagonal lattice diffraction with a 540-Å unit cell constant. Since the diffraction spots do not broaden with reciprocal lattice spacing, the long-range order is good. Repeating structures along the axes of the microvilli give rise to arcs at $(90\ Å)^{-1}$ and $(53\ Å)^{-1}$ along the horizontal axis of the pattern. Fig. 2 *b* is a more intense exposure (due to the inverse-square dependence on sequence-to-film distance), showing the continuous scatter that coincides with the lattice reflections and extends into additional diffuse features in the outer part of the pattern. The six outer diffuse maxima, outlined in one sector,

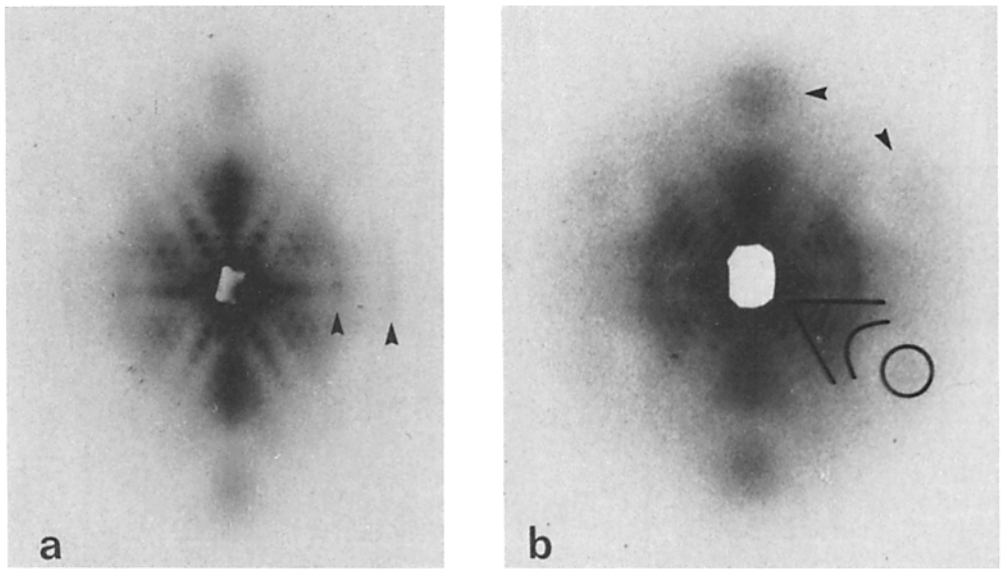

Figure 2. Low-angle X-ray diffraction patterns of glutaraldehyde-fixed slices of squid retina. These patterns are the sum of diffraction from two orthogonally oriented sets of microvilli whose diffraction axes are shown in Fig. 1 (*right*). (*a*) 40-h exposure at a specimen-to-film distance of 23 cm. Diffraction peaks due to the 540-Å hexagonal lattice of microvilli (viewed as in Fig. 3 *a*) and superimposed diffuse scatter make up the characteristic intensity distribution of the rhabdome structure. Arrowheads indicate diffraction arcs from longitudinal repeats (microvilli viewed as in Fig. 3 *b*) of $(90\ Å)^{-1}$ and $(53\ Å)^{-1}$ along the microvillar axes. (*b*) A 20-h exposure at 12-cm specimen-to-film distance. The stronger exposure brings up the diffuse scatter in the outer part of the pattern. Arrowheads indicate diffuse maxima centered around $(40\ Å)^{-1}$, one of which is circled. The intensity is stronger on the vertical axis of the pattern because the "sideways-oriented" microvilli (as in Fig. 3 *b*) add vertically projected diffraction to the hexagonally symmetric diffraction from the head-on microvilli. Diffuse tails of intensity extend from the more central parts of the pattern to partially encircle the $(40\ Å)^{-1}$ maxima. On one sector of the pattern, the triangular area and projecting diffuse tails are outlined, together with the $(40\ Å)^{-1}$ maximum.

are centered at (40 Å)$^{-1}$ and originate from the headgroup separation of the phospholipid bilayer (34). They are diffuse spots rather than a diffuse ring because the microvilli are not circular in profile, but are rounded hexagons (this shape can be seen in Fig. 3, *c* and *d*). Note the diffuse extensions of the triangular regions that form a partial frame around the (40 Å)$^{-1}$ maxima (Fig. 2 *b*).

The use of glutaraldehyde-fixed retina is unlikely to have altered the membrane bilayer profile: as long as the osmotic balance of the fixative is correct, the effect of glutaraldehyde on the electron density profile is mainly to alter the gaps between closely apposed membranes (1, 11). It is however likely to cause aggregation of cytoskeletal structures.

Electron Microscopy and Image Analysis of the Microvillar Lattice

Thin section electron micrographs of squid photoreceptor microvilli reveal a highly ordered membrane array with less well-ordered cytoskeletal components in the microvillar cytoplasm (Fig. 3). This structure is found through most of

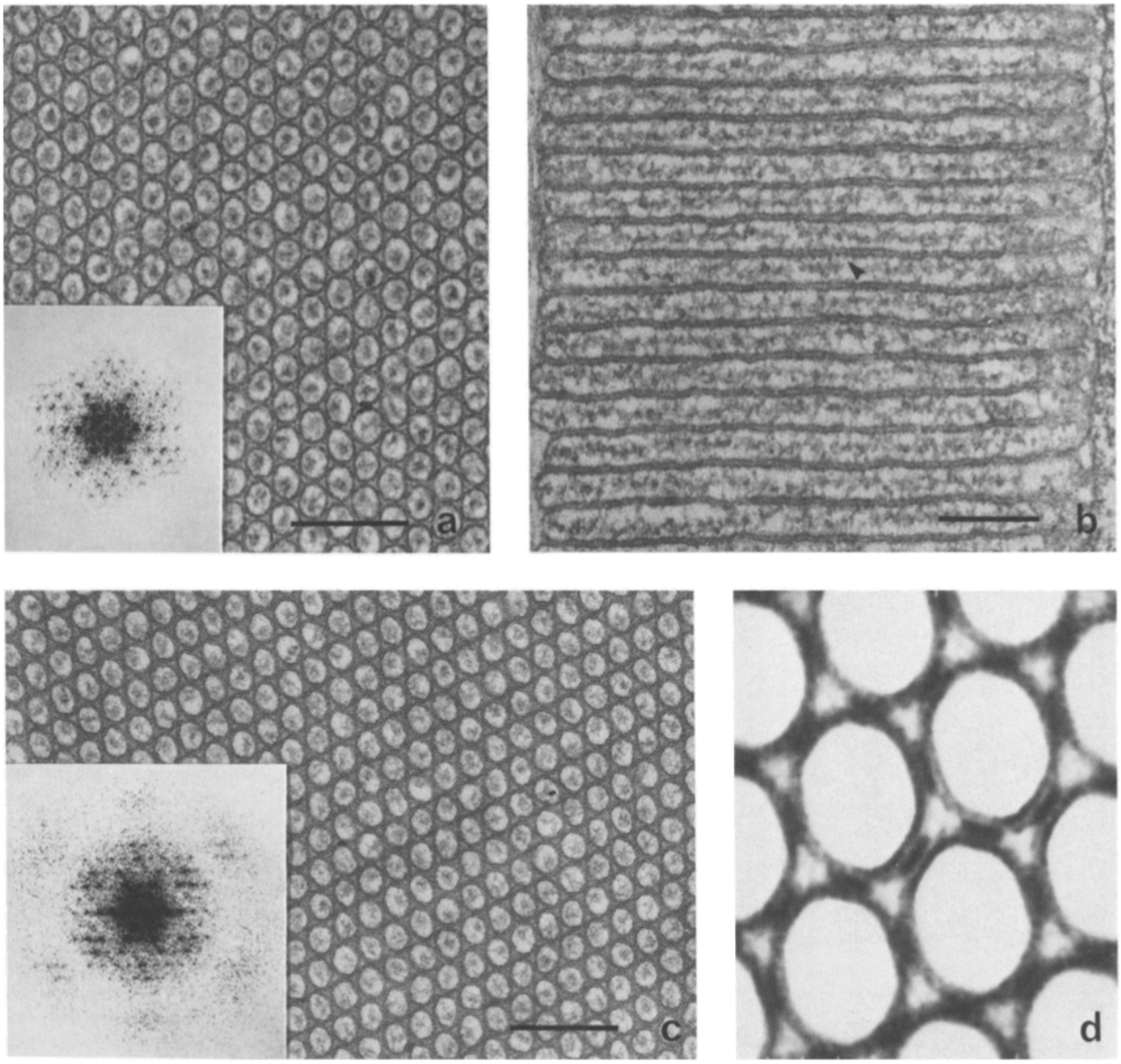

Figure 3. Electron microscope sections and image analysis of photoreceptor microvilli fixed in the presence of sucrose. (*a*) Cross section of the 540-Å lattice of closely apposed microvillar membranes, stained with phosphotungstic acid, which does not give bilayer staining of membranes but stains the cytoskeleton relatively strongly. (*Inset*) The computed diffraction pattern from an area of this section containing 150 microvilli. (*b*) An adjacent area of longitudinally sectioned microvilli, stained with phosphotungstic acid, showing their full 1-μm length. They join the central column of retinula cell cytoplasm (*right*) through narrow necks of membrane. The arrowhead indicates a region of striations that appear to cross the membrane pair and extend into surface granularities. (*c*) A similar section stained with uranyl acetate and lead citrate showing the bilayer structure of the membranes. (*Inset*) The computed diffraction pattern from 150 microvilli. In addition to the central hexagonal lattice diffraction, diffuse maxima centered around (55 Å)$^{-1}$ arise from the bilayer staining. (*d*) A real space correlation average of 86 microvilli from *c* showing the dense stain in the membrane junctions and hints of a threefold structure in the interstices between microvilli. The cytoskeleton is disordered and is smoothed out by averaging. The lattice is distorted from true hexagonal symmetry during processing for embedding and sectioning. No symmetry assumptions are applied in this and Fig. 4. Bars, 0.2 μm.

the depth of the squid retinal photoreceptor layer with the exception of a thin surface layer in which the microvilli are disordered and appear to be undergoing degradation (data not shown). The cytoskeleton is strongly stained with phosphotungstic acid, which does not reveal the bilayer nature of membranes but appears to stain mainly protein components (Fig. 3, *a* and *b*). The diffraction pattern computed from this micrograph (Fig. 3 *a*, *inset*) resembles the X-ray patterns but lacks the bilayer maxima. Long sections of the microvilli (Fig. 3 *b*) show the filamentous core that is likely to be an aggregate of 2–3 actin filaments (4, 30) and a series of sidearms linking the filaments to the membranes. A surface granularity with a periodicity of ~120 Å is discernible on the cytoplasmic side of the membranes, and may represent sites of membrane-cytoskeleton attachment (see *arrow*, Fig. 3 *b*).

Conventional section staining with uranyl acetate and lead citrate gives characteristic bilayer staining (Fig. 3 *c*). The computed diffraction pattern (*inset*) more closely resembles the X-ray pattern, including diffuse maxima centered around $(55\ \text{Å})^{-1}$ (vs. $[40\ \text{Å}]^{-1}$ for X-ray). In the correlation-averaged image of this section (Fig. 3 *d*), a dense layer of staining along the membrane pair contact region is a prominent feature. These membrane junctions are retained under a wide range of fixation conditions involving significant shape changes in the microvilli (data not shown). The microvilli are never seen detached from one another, except in the disordered surface layer mentioned above. The cytoskeletons are weakly stained and disordered, and they become smoothed out in the averaged image (Fig. 3 *d*).

Fixation of the retinas in the presence of high molecular mass (70 but not 40 kD) dextrans reveals fine substructure of the intermembrane contacts not previously visible (Fig. 4 *a*). However the microvilli are irregularly swollen and too disordered for image analysis. They are shortened and wid-

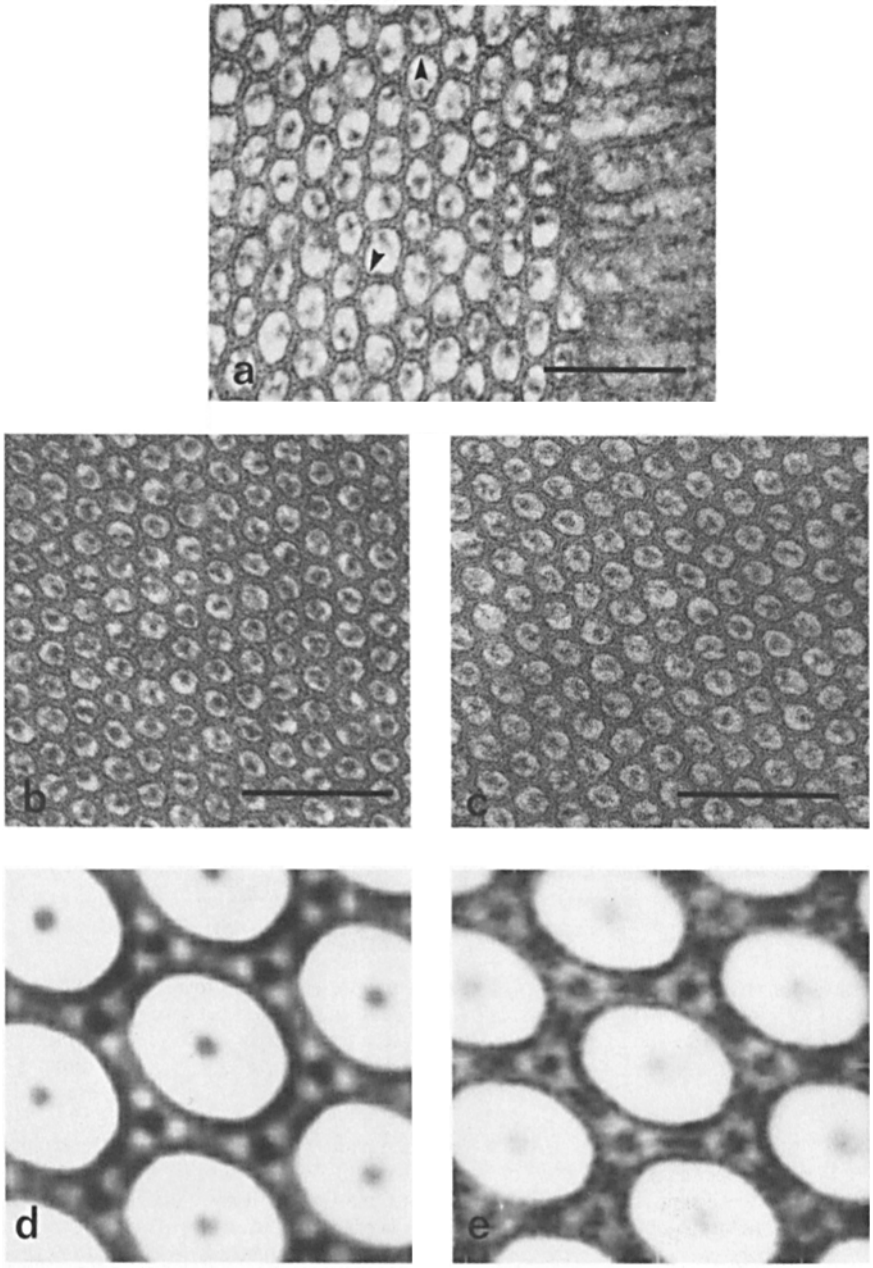

Figure 4. Electron microscope sections and image averaging of retinas fixed in the presence of high molecular weight dextran. (*a*) Swollen and disordered microvilli fixed in dextran-containing solutions and stained with phosphotungstic acid. Fine striations are visible between the apposed membranes, indicating the preservation of membrane substructure. The appearance of two- and three-stranded structures is indicated by the upper and lower arrowhead, respectively. (*b* and *c*) Phosphotungstic acid and uranyl-lead–stained sections of microvilli fixed in solutions containing both sucrose and dextran. They are less swollen and the lattice order is sufficient for real space image averaging. (*d* and *e*) Correlation averages of *b* and *c*, respectively. The phosphotungstic acid average of 256 microvilli (*d*), sampled at intervals of 22 Å (by scanning the micrograph at 100 μm on the densitometer), shows a prominent Y-shaped feature at the threefold contacts between microvilli and the twofold junction sometimes appears to be resolved into two strands (e.g., top and right of central microvillus). (*e*) The uranyl acetate-lead citrate–stained section contains finer details and was sampled at 16 Å (by interpolation of a 50-μm densitometer scan). The average of 155 microvilli also reveals the threefold structure, and the twofold junctions appear to traverse both bilayers. The cytoskeleton is smeared out in these averages to a faint diffuse blob at the center of each microvillus. Bars, 0.2 μm.

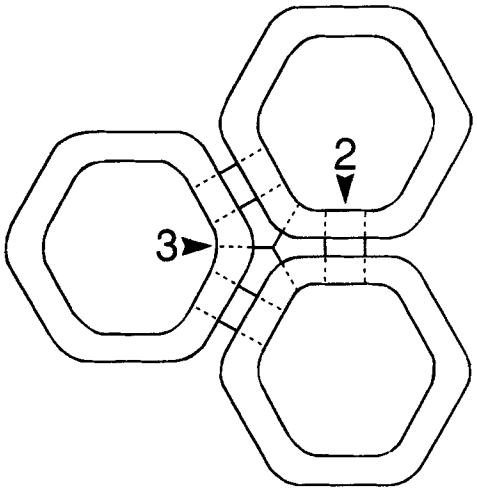

Figure 5. Schematic representation of the junctions at twofold and threefold positions between microvilli. The averages in Fig. 4, *d* and *e*, suggest that the junctions are transmembrane densities.

ened, but despite these shape changes the membrane junctions are retained, presumably by rearrangement of components in the plane of the membrane. Combining high molecular weight dextrans with sucrose yields narrower and more uniform microvilli (Fig. 4, *b* and *c*). In this case the images are less distinct but new features can be resolved by correlation averaging. Averaged images of such phosphotungstic acid-stained sections show distinct three-way junctions at the threefold positions and resolve the membrane pair contacts into two principal strands of density (Fig. 4 *d*). A schematic representation of the two- and threefold junctions is given in Fig. 5. They are also seen in the uranyl-lead-stained sections (Fig. 4 *e*). As above, the cytoskeleton is weak and disordered and gets smeared out in the averaged image, while the membrane junction regions are relatively well-ordered and appear more distinct in the averaged image. The structure in the presence of high molecular weight dextran also differs in the longitudinal repeats seen by X-ray diffraction (data not shown). The 90-Å axial repeat is replaced by 72- and 65-Å repeats, while the 53-Å axial reflection, tentatively attributed to rhodopsin (18), is unchanged.

Disorder in the Microvillar Lattice. X-ray diffraction patterns from squid photoreceptors contain a mixture of discrete spots from the hexagonal lattice and diffuse features from disordered structures. In the image transforms, as well as in the X-ray patterns, the Bragg spots fade rapidly but do not broaden with reciprocal lattice spacing and the distribution of diffuse scattering in the outer part of the pattern is a smooth continuation of the Bragg intensities. This can be explained by reference to the original images. The lattice directions are preserved over long distances but the microvilli are locally variable in shape and size. This means that the long range order is good but the short range order is poor. In other words, wider microvilli tend to be neighbored by narrower ones. The continuous diffraction is thus produced by scattering from oriented membrane pairs with variable positions in the unit cell. The adjoining membranes act as a unit since they are firmly bound together by the twofold junctions but other parts of the membrane are deformable. Thus the Bragg and diffuse scattering intensity distributions are similar because they arise from the same objects, correlated in space at low resolution (near the center of the diffraction pattern, corresponding to large spacings in the structure) to give the Bragg spots and uncorrelated at higher resolution (towards the periphery of the diffraction pattern, corresponding to finer details in the structure) to give the diffuse scattering. Real space correlation averaging (see Materials and Methods) incorporates this higher resolution information while Fourier filtering techniques do not.

Model Calculations of the Electron Density Map

In principle, X-ray diffraction gives a faithful picture of the electron density of a structure since it arises from hydrated, unstained specimens. However, its interpretation is indirect and we have sought a solution by model building. We have constructed electron density maps of the microvillar cross section using information from electron microscopy and chemical composition in order to reproduce the major intensity maxima and minima seen in the observed X-ray patterns. For ease of calculation, a perfect hexagonal lattice was assumed, but the lattice sampling was ignored when comparing intensity features in the models and data. To evaluate the models, the positions of major maxima and minima in the calculated intensities were compared with those in the observed patterns. The justification for treating Bragg and continuous diffraction together is given in the previous section. The X-ray intensities were not corrected by a Lorentz factor for mosaic spread or the model intensities by a Debye-Waller factor for spatial disorder. Since these are both radial corrections that tend to cancel one another we did not consider this necessary for the semi-quantitative comparisons being made.

The similarity between the X-ray patterns (Fig. 2) and the electron micrograph transform (Fig. 3 *c inset*) suggests that, to a first approximation, the real electron density distribution in the microvilli resembles that of the electron scattering stain. However the resemblance is less strong in the higher resolution (outer) region of the pattern, where the diffuse maxima are at different spacing in X-ray and EM, and the diffuse tails noted in the X-ray pattern (Fig. 2 *b*) are absent from the micrograph transform. We therefore set out to construct a physically and biochemically reasonable model for the electron density map that would fit the higher resolution X-ray intensities. We found that the diffraction pattern is essentially determined by the structure of the membrane pair.

The microvillar membranes contain about equal amounts of rhodopsin and phospholipid, as do ROS disc membranes, in addition to other proteins and cholesterol in the invertebrate system (15). One might therefore expect the experimentally determined electron density profile of the disc membrane to give a reasonable model. This profile is shown in Fig. 6, in relation to the pair of phospholipid bilayers it represents. As previously reported (18), the diffraction pattern of such models does not fit the data, but shows a very pronounced intensity minimum in a region where the X-ray intensity is strong (compare Fig. 7 *a* with Fig. 2). Finding a model to fit the data was greatly facilitated by the fact that the radial positions of the broad intensity minimum and the outer diffuse maxima (these are indicated on the diagram in Fig. 7 *g*) are largely determined by two parameters whose values can be independently optimized. These are intermem-

brane separation and the shape of the membrane electron density profile (expressed as the ratio of electron density in the headgroup peaks to that in the hydrophobic minimum). A less important parameter is the degree of flattening of the microvillus, which sharpens the outer diffuse maxima. This depends on the fixation conditions. Finally, an important parameter is the headgroup peak separation but the value of this is determined by the distribution of phospholipid chain lengths. This distribution is very similar to that of disc membrane and a peak separation of 40–45 Å is used in the models. Variations within this range do not significantly affect the model diffraction patterns.

Membrane Profile and Pair Separation. The model diffraction patterns and corresponding profiles in Fig. 7, *a–c*, show the effect of varying the electron density profile of the microvillar membrane. The profile in Fig. 7 *a* corresponds to that of ROS disc membrane, while Fig. 7 *b* resembles the bilayer part of gap junction membrane (13). We found it necessary to fill in the hydrophobic trough still further (Fig. 7 *c*) in order to fit the position of the observed X-ray intensity minimum ($\sim$[60 Å]$^{-1}$). In Fig. 7, *d–f*, the center to center separation of the membrane pairs was varied from 65 to 85 Å. The best fit for the position of the outer diffuse X-ray maxima ([40 Å]$^{-1}$) is a separation of 75 $\pm$ 5 Å.

Density Variations in the Plane of the Membrane. The faint but distinctive streaks of X-ray intensity in the region of the (6, 2), (7, 2), and (8, 2) Bragg reflections (equivalent to the diffuse tails noted in Fig. 2 *b*) were never observed in electron micrograph transforms (Fig. 3) or in the basic model patterns (Fig. 7). We were unable to find a model whose diffraction pattern would reproduce the observed intensity in this region. We took the approach of increasing amplitudes for the (6, 2), (7, 2) and symmetry-related reflections (assuming 6mm symmetry) in the best model pattern (Fig. 7 *e*) in order to see what effect these intensities could have on the structure. There are four possible phase combinations that can be used to calculate the structure modified by the addition of these two reflections. All four had the principal effect of causing variations in electron density around the perimeter of the microvillus. Two of the phase combinations generated threefold junctions in the interstices similar to those observed by EM (Fig. 4). One of these, +(6, 2), −(7, 2), gave a set of three transmembrane densities at the membrane pair contacts, and the other (−, −) gave two major transmembrane densities and two intermicrovillar densities. This was judged to be in best agreement with the averaged images (Fig. 4, *d* and *e*). The final model was arrived at by alternately smoothing out density variations in the microvillar cytoplasm to the solvent level and increasing the negative (6, 2) and (7, 2) amplitudes. The final electron density models and their diffraction patterns are shown for circular and hexagonal microvilli in Fig. 8. The electron density maps show the three-way junctions and 2–4 strands of density crossing the membrane pair contacts. The best fit to the X-ray patterns (Fig. 2) is the flattened model pattern in Fig. 8 *d*.

Protein Composition of the Microvillar Membranes

The microvillar polypeptide composition is shown in Fig. 9 (*M*) and is resolved into detergent (octyl glucoside) soluble (*S*) and pellet (*P*) fractions. Densitometry of the gel lanes shows that $\sim$50% of the total protein is rhodopsin. Part of the diffuse 45-kD rhodopsin band is composed of other protein, notably the α-subunit of GTP-binding protein (20, 31). 70% of the total protein is detergent soluble with rhodopsin and the 47- and 190-kD components being the major glycoproteins (unpublished observations). The 35-kD component is thought to be the β-subunit of GTP-binding protein, based on antibody cross-reactivity studies (28). Of the remaining 30% of detergent insoluble protein comprising four major polypeptides, only actin has been identified (18).

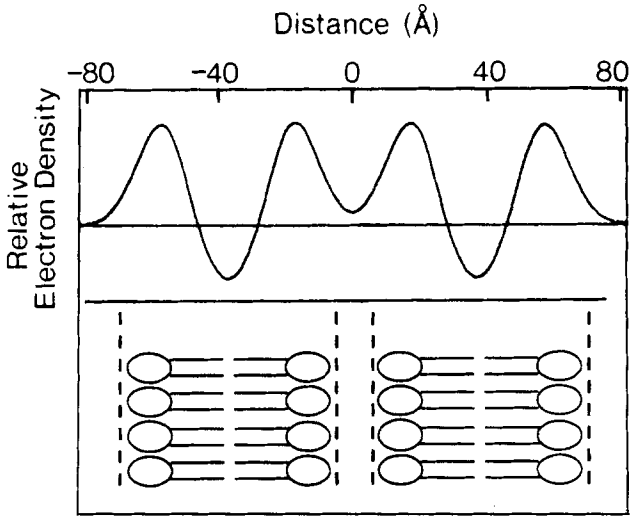

Figure 6. The electron density profile of ROS disk membrane taken from the data of Chabre (2) and positioned at the spacing of the membrane pairs in squid photoreceptors. The peaks correspond to the phospholipid headgroups and the troughs to the hydrocarbon chain regions of the schematic bilayers shown below.

Discussion

Protein Content in the Bilayer

The diffraction results imply a surprisingly high protein content in the hydrophobic layer of the microvillar membrane, as well as a dense array of surface projections, some of which are likely to be extensions of transmembrane densities. The model calculations (Fig. 7, *a–c*) show that the X-ray pattern is extremely sensitive to the shape of the bilayer electron density profile, which is itself very sensitive to the hydrophobic protein content. In the ROS disc membrane the rhodopsin content is $\sim$50%. About one-third of its amino acid residues project into the aqueous phases (Findlay, in reference 25), giving a hydrophobic protein content of $\sim$40%. Increasing the hydrophobic protein content to 50%, the value estimated for gap junction membrane (13, 29) fills the central trough in the bilayer profile up to the water electron density level. However, the profile that best fits the observed X-ray pattern of squid photoreceptor membranes (Figs. 7 *e* and 8 *b*) is even more filled in than the gap junction profile. This implies a hydrophobic protein content somewhat greater than 50%.

This might be achieved by a higher density of rhodopsin packing and/or a substantial amount of additional transmembrane protein in squid photoreceptor membrane as compared with ROS disc membrane. Since the rhodopsin/lipid ratio is if anything slightly lower than that in ROS (15), a substantial part of the nonrhodopsin protein is required to penetrate through the bilayer to account for the electron density map.

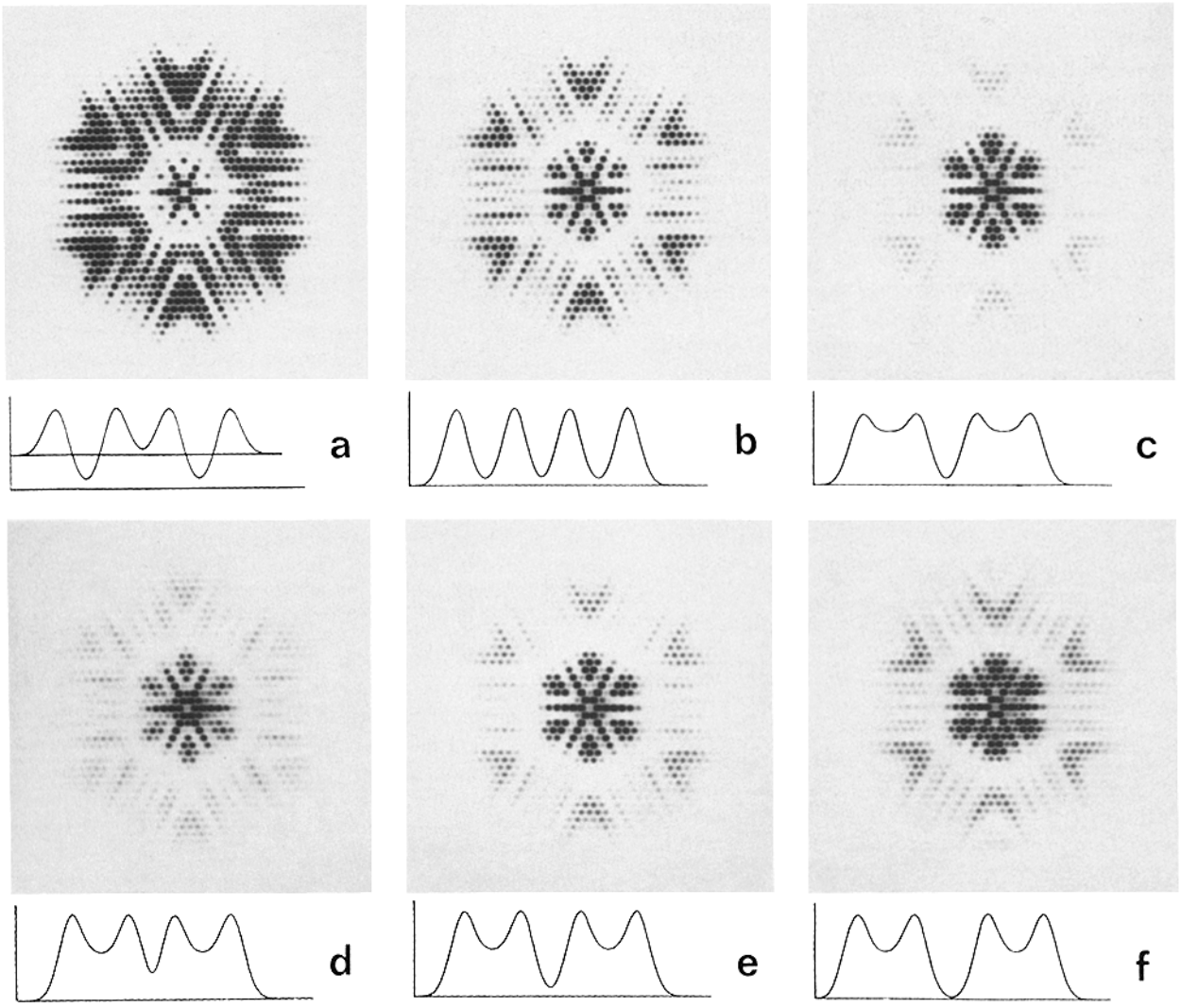

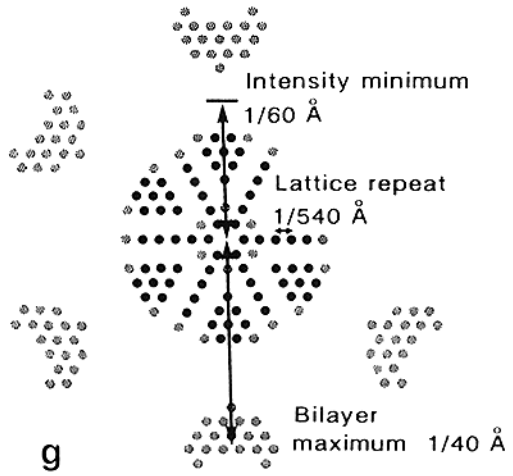

Figure 7. Model diffraction patterns and membrane pair electron density profiles. Models were constructed in which membranes of varying electron density profile and pair separation were assembled into the hexagonal array of microvilli. The microvillus cross section was a rounded hexagon as in Fig. 8 *b*. The highest resolution terms in the models corespond to 36-Å spacing. Diffraction patterns are shown for a series of six models, together with a linear electron density profile of the membrane pair. (*a–c*) Calculated diffraction patterns and membrane profiles for microvilli with a membrane pair separation of 75 Å and a variable membrane profile. (*a*) Profile based on a pair of ROS disc membranes. The experimentally determined profile shows a pair of electron dense phosphate headgroups, separated by 42 Å, with a trough going below the solvent electron density level, at the center of the bilayer. The diffraction pattern shows a pronounced intensity minimum around $(110\ \text{Å})^{-1}$. (*b*) Profile based on the bilayer part of gap junction membrane. The central trough is at the solvent level, and the diffraction intensity minimum has moved out to about $(80\ \text{Å})^{-1}$. (*c*) A very filled-in membrane profile resembling that of *Halobacterium* purple membrane. The intensity minimum is around $(60\ \text{Å})^{-1}$. (*d–f*) Profiles with a trough/peak ratio of 1:2 and variable membrane separation. (*d*) Membrane center–center distance of 65 Å. The diffuse bilayer intensity maxima are centered at $(36\ \text{Å})^{-1}$. (*e*) Membrane separation 75 Å, bilayer maxima at $(40\ \text{Å})^{-1}$. (*f*) Membrane separation 85 Å, bilayer maxima at $(47\ \text{Å})^{-1}$. (*g*) The scales and positions of the intensity features being modeled.

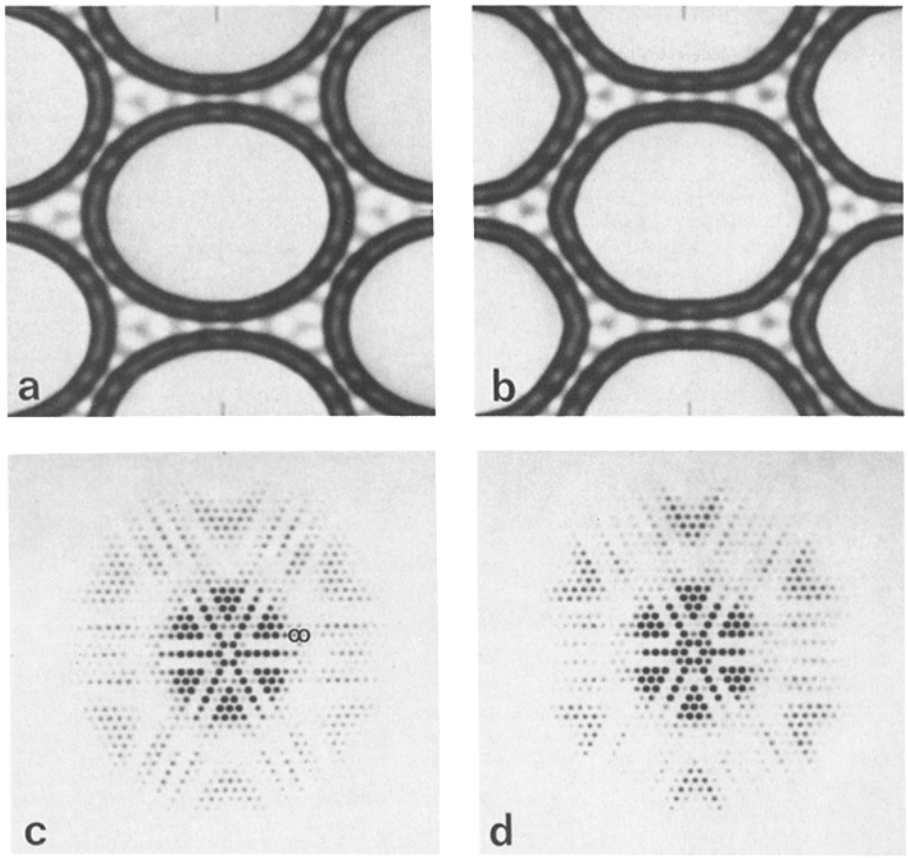

Figure 8. Model electron density maps and diffraction patterns with added (6, 2) and (7, 2) reflections, with phases (−, −). The 15% compression along the vertical axes of the models is due to the computation method, explained in Materials and Methods. It causes slight variations in different directions on the diffraction patterns. (*a*) Round and (*b*) hexagonal microvillus models with membrane profile and separation as in Fig. 7 *e*. (*c* and *d*) The corresponding diffraction patterns. The (6, 2) and (7, 2) reflections are circled in *c* and correspond to the diffuse tails of intensity noted in Fig. 2 *b*, which are absent from all the model patterns in Fig. 7. Density variations resulting from the added reflections are the Y-shaped threefold junctions and 2–4 strands of density crossing both membranes at the pair contacts. The highest resolution terms in the models correspond to a spacing of 36 Å.

This conclusion is not affected by considerations of the cytoskeletal and membrane junction structures. The cytoskeleton is a weak and disordered feature that only affects the very low resolution part of the pattern ($\leq 1/540\,\text{Å}^{-1}$). The density fluctuations associated with the membrane junctions are also relatively weak and do not affect the principal maxima and minima of diffracted intensity. Furthermore, uncertainty in the electron density level of the extracellular and cytoplasmic fluid is unlikely to account for overestimation of the hydrophobic protein content as similar X-ray patterns have been recorded in sucrose concentrations ranging from 10–30% (wt/vol) (18, and unpublished data).

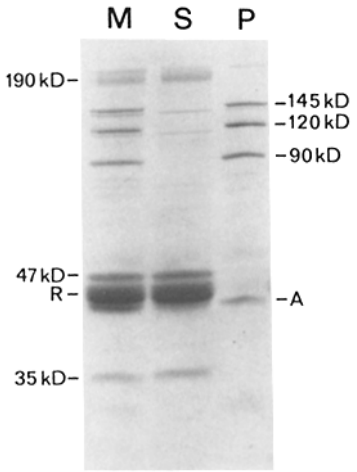

Figure 9. SDS PAGE of the microvillar membrane and cytoskeleton proteins. (*M*) Total proteins in isolated photoreceptor microvilli; (*R*) rhodopsin (molecular mass 45 kD); (*S*) detergent soluble components; (*P*) detergent pellet. (*A*) actin. Molecular masses are interpolated from the migration positions of the following markers: myosin, 205 kD; β-galactosidase, 116 kD; phosphorylase, 97 kD; ovotransferrin; 77 kD; BSA, 67 kD; ovalbumin, 45 kD; transducin α-subunit 39 kD; transducin β-subunit, 35 kD.

Surface and Transmembrane Structures

Transmembrane links of the type reported here were first seen in sections of mosquito photoreceptors, although in a very disordered form (33), and threefold structures at the microvillar interstices in honeybee retina have also been observed (16). These structures repeat along the microvillar axis, with periodicities of 70–200 Å, on the basis of long sections (Fig. 3 *b*) and the axial X-ray reflections (Fig. 2 and unpublished observations). Many rearrangements can take place during fixation. The microvilli are very variable in length and diameter and in axial repeat distances. Although the twofold junctions are always seen, the threefold structures are only observed under favorable fixation conditions. The density of surface projections could approach the expected rhodopsin separation distance of 50–60 Å. It is very unlikely, however, that the intermicrovillar contacts are composed of rhodopsin molecules because *Drosophila* mutants lacking rhodopsin can have a normal microvillar structure (24). Other polypeptides present in sufficient quantity to account for these structures are the detergent soluble 47- and 190-kD components, and the detergent insoluble proteins between 90 and 145 kD (Fig. 9).

Implications of the Structure for the Optical, Electrical, and Mechanical Properties of Rhabdomes

The locally deformable network provides long range order in the microvillar array, ensuring the correct orientation of microvilli for absorption of light and the orthogonal packing necessary for polarization sensitivity over the surface of the retina. The high membrane protein content and the dense ar-

ray of microvillar surface projections must present a substantial barrier to rhodopsin mobility. This explains the long standing observations of high polarization sensitivity and dichroism that require a high degree of rhodopsin alignment in the plane of the microvillar membrane (6, 7, 26).

The close apposition of microvillar membranes (75 Å center-to-center of the membrane pairs) gives a high resistance to extracellular current flow through the rhabdome. The gap between adjacent membranes may be as little as 15 Å, as compared with 30 Å in gap junctions, which appear to have a thicker extracellular layer in EM sections (1). It has been suggested on the basis of response kinetics in fly rhabdomes that the light-activated sodium conductances are in the loop region formed by the necks of the microvilli (8). In the squid, this would appear to be the only region where there is an appreciable volume of extracellular space. To carry out its photoreceptor function, the microvillar array must provide the membrane matrix on which phototransduction enzymes can diffuse and interact with rhodopsin and other proteins. The junctions at the two- and threefold positions define ordered domains that may play a role in aligning the rhodopsin molecules. It will be of great interest to identify and characterize the proteins involved in the membrane surface interactions that give these microvilli their unique structural and mechanical properties.

We thank the Marine Biological Association (Plymouth, UK) for the excellent supply of squid and research facilities. We are grateful for the expert assistance of Mr. T. Rutherford of King's College London for the construction and maintainance of X-ray diffraction equipment, and of Mr. Z. Gabor for the photography of X-ray patterns. We thank Dr. Garry Taylor for help with all aspects of computing, Dr. Owen Saxton for installing the SEMPER system, Dr. H. D. Middendorf for devising an early version of the model calculation program, Drs. D. L. D. Caspar and N. Franks for discussions, Drs. W. Kühlbrandt, H. D. Middendorf, R. Wade, and Mr. N. White for comments on the manuscript, and Mr. Martin Lomas for help with sectioning.

This work was supported by the United Kingdom Medical Research Council and by the European Molecular Biology Organization.

Received for publication 29 September 1986, and in revised form 12 February 1987.

References

1. Caspar, D. L. D., D. A. Goodenough, L. Makowski, and W. C. Phillips. 1977. Gap junction structures. I. Correlated electron microscopy and X-ray diffraction. *J. Cell Biol.* 74:605–628.
2. Chabre, M. 1975. X-ray diffraction studies of retinal rods. 1. Structure of the disc membrane, effect of illumination. *Biochim. Biophys. Acta.* 382:322–335.
3. Cincotta, D., and W. Hubbell. 1977. Freeze-fracture studies of squid photoreceptor membranes. *Invest. Ophthalmol. & Visual Sci.* (Suppl.) 165.
4. de Couet, H. G., S. Stowe, and A. D. Blest. 1984. Membrane-associated actin in the rhabdomeral microvilli of crayfish photoreceptors. *J. Cell Biol.* 98:834–846.
5. Fernandez, H. R., and E. E. Nickel. 1976. Ultrastructural and molecular characteristics of crayfish photoreceptor membranes. *J. Cell Biol.* 69: 721–732.
6. Foster, M. C. 1980. Solution of the diffusion equation for membranes containing microvilli and lateral diffusion of rhodopsin and lipid analogs in squid photoreceptor membranes. *Fed. Proc.* 39:2067.
7. Goldsmith, T., and R. Wehner. 1977. Restrictions on rotational and translational diffusion of pigment in the membranes of a rhabdomeric photoreceptor. *J. Gen. Physiol.* 70:453–490.
8. Hamdorf, K., and K. Kirschfeld. 1980. "Prebumps": evidence for double-hits at functional subunits in a rhabdomeric photoreceptor. *Z. Naturforsch.* 35c:173–174.
9. Hewat, E. A., S. Cusack, H. Ruigrok, and C. Verwey. 1984. Low resolution structure of the influenza virus C glycoprotein determined by electron microscopy. *J. Mol. Biol.* 175:175–193.
10. Johnson, E., P. Robinson, and J. Lisman. 1986. Involvement of cGMP in the excitation of invertebrate photoreceptors. *Nature (Lond.).* 324:468–470.
11. Kirschner, D. A., and C. J. Hollingshead. 1980. Processing for electron microscopy alters membrane structure and packing in myelin. *J. Ultrastruct. Res.* 73:211–232.
12. Laemmli, U. K. 1970. Cleavage of structural proteins during the assembly of the head of bacteriophage T4. *Nature (Lond.).* 227:680–685.
13. Makowski, L., D. L. D. Caspar, W. C. Phillips, and D. A. Goodenough. 1977. Gap junction structures. II. Analysis of the X-ray diffraction data. *J. Cell Biol.* 74:629–645.
14. O'Tousa, J., W. Baehr, R. Martin, J. Hirsh, W. Pak, and M. Applebury. 1985. The *Drosophila* ninaE gene encodes an opsin. *Cell.* 40:839–850.
15. Paulsen, R., D. Zinkler, and M. Delmelle. 1983. Architecture and dynamics of microvillar photoreceptor membranes of a cephalopod. *Exp. Eye Res.* 36:47–56.
16. Perrelet, A., and F. Baumann. 1969. Evidence for extracellular space in the rhabdome of the honeybee drone eye. *J. Cell Biol.* 40:825–830.
17. Roof, D., and J. Heuser. 1982. Surfaces of rod photoreceptor disk membranes: Integral membrane components. *J. Cell Biol.* 95:487–500.
18. Saibil, H. R. 1982. An ordered membrane-cytoskeleton network in squid photoreceptor microvilli. *J. Mol. Biol.* 158:435–456.
19. Saibil, H. R. 1984. A light-stimulated increase of cyclic GMP in squid photoreceptors. *FEBS (Fed. Eur. Biochem. Soc.) Lett.* 168:213–216.
20. Saibil, H. R., and M. Michel-Villaz. 1984. Cross-reactions between rhodopsin and GTP-binding protein in bovine and squid photoreceptors. *Proc. Natl. Acad. Sci. USA.* 81:5111–5115.
21. Saxton, W. O. 1978. Computer techniques for image processing in electron microscopy. Academic Press, Inc., New York, N.Y. 41–43.
22. Saxton, W. O., and W. Baumeister. 1982. The correlation averaging of a regularly arranged bacterial cell envelope protein. *J. Microsc. (Oxf.)* 127:127–138.
23. Saxton, W. O., T. J. Pitt, and M. Horner. 1979. Digital image processing: the Semper system. *Ultramicroscopy.* 4:343–354.
24. Schinz, R., M.-V. Lo, D. Larrivee, and W. Pak. 1982. Freeze-fracture study of the *Drosophila* photoreceptor membrane: mutations affecting particle density. *J. Cell Biol.* 93:961–969.
25. Stieve, H. 1986. The Molecular Mechanism of Photoreception. Springer-Verlag, GmbH & Co., Berlin.
26. Sugawara, K., Y. Katagiri, and T. Tomita. 1971. Polarized light responses from *Octopus* single retinular cells. *J. Fac. Sci. Hokkaido Univ. Ser. VI Zool.* 17:581–586.
27. Szuts, E., S. Wood, M. Reid, and A. Fein. 1986. Light stimulates the rapid formation of inositol trisphosphate in squid retinas. *Biochem. J.* 240: 929–932.
28. Tsuda, M., T. Tsuda, Y. Terayama, Y. Fukada, T. Akino, G. Yamanaka, L. Stryer, T. Katada, M. Ui, and T. Ebrey. 1986. Kinship of cephalopod photoreceptor G-protein with vertebrate transducin. *FEBS (Fed. Eur. Biochem. Soc.) Lett.* 198:5–10.
29. Unwin, P. N. T., and P. D. Ennis. 1984. Two configurations of a channel forming membrane protein. *Nature (Lond.).* 307:609–613.
30. Usukura, J. 1984. International Congress on Cell Biology of Photoreceptors, Tokyo.
31. Vandenberg, C. A., and M. Montal. 1984. Light regulated biochemical events in invertebrate photoreceptors. 1. Light-activated guanosinetriphosphatase, guanine nucleotide binding, and cholera toxin catalyzed labelling of squid photoreceptor membranes. *Biochemistry.* 23:2339–2347.
32. Vandenberg, C. A., and M. Montal. 1984. Light regulated biochemical events in invertebrate photoreceptors. 2. Light regulated phosphorylation of rhodopsin and phosphoinositides in squid photoreceptor membranes. *Biochemistry.* 23:2347–2352.
33. White, R. W. 1967. The effect of light and light deprivation upon the ultrastructure of the larval mosquito eye. *J. Exp. Zool.* 166:405–426.
34. Wilkins, M. H. F., A. E. Blaurock, and D. M. Engelman. 1971. Bilayer structure in membranes. *Nature New Biol.* 230:72–76.
35. Yoshioka, T., H. Inoue, M. Takagi, F. Hayashi, and T. Amakawa. 1983. The effect of isobutylmethylxanthine on the photoresponse and phosphorylation of phosphatidylinositol in *Octopus* retina. *Biochim. Biophys. Acta.* 755:50–55.